4D Corneal Tissue Engineering: Achieving Time-Dependent Tissue Self-Curvature through Localized Control of Cell Actuators

*Martina Miotto, Ricardo M. Gouveia, Ana M. Ionescu, Francisco Figueiredo, Ian W. Hamley and Che J. Connon**

Dr. M. Miotto, Dr. R.M. Gouveia, Prof. F. Figueiredo and Prof. C.J. Connon

Institute of Genetic Medicine, Newcastle University, International Centre for Life, Central Parkway, Newcastle upon Tyne, NE1 3BZ, United Kingdom

Prof. F. Figueiredo

Department of Ophthalmology, Royal Victoria Infirmary, Queen Victoria Road, Newcastle upon Tyne, NE1 4LP, United Kingdom

Prof. I.W. Hamley

School of Chemistry, Food and Pharmacy, University of Reading, Whiteknights, Reading RG6 6UB, United Kingdom

Dr. A.M. Ionescu

Departamento de Óptica, Facultad de Ciencias, Universidad de Granada, Avenida de la Fuente Nueva S/N C.P. 18071, Granada, Spain

Prof. C.J. Connon

E-mail: Che.Connon@newcastle.ac.uk

Keywords: 4D tissue engineering, bio-actuators, cell-driven tissue curvature, peptide amphiphiles, artificial corneal stroma

Abstract

While tissue engineering is widely used to construct complex tridimensional biocompatible structures, researchers are now attempting to extend the technique into the fourth dimension. Such fourth dimension consists in the transformation of 3D materials over time, namely by changing their shape, composition, and/or function when subjected to specific external stimuli. In this study, we instead explored producing a 4D biomaterial with an internal mechanism of stimulus, using contractile cells as bio-actuators to change tissue shape and structure. Specifically, we aimed at producing cornea-shaped, curved stromal tissue equivalents via the controlled, cell-driven curving of collagen-based hydrogels. This was achieved by modulating the activity of the bio-actuators in delimited regions of the gels using a contraction-inhibiting peptide amphiphile. The self-curved constructs were then characterized in terms cell and collagen fibril re-organization, gel stiffness, cell phenotype, and the ability to sustain the growth of a corneal epithelium *in vitro*. Overall, our results showed that the structural and mechanical properties of self-curved gels acquired through a 4D engineering method were more similar to those of the native tissue, and represented a significant improvement over planar 3D scaffolds. In this perspective, this study demonstrates the great potential of cell bio-actuators for 4D tissue engineering applications.

1. Introduction

In the past few decades, considerable efforts have been made to engineer new biomaterials that successfully emulate the complex three-dimensional (3D) organization of human tissues in order to better replace them. These 3D tissue equivalents are commonly comprised of natural or synthetic components designed to reproduce the structure and mechanics of native extracellular matrix (ECM) and provide suitable biochemical and biophysical cues for supporting the adhesion, growth, and survival of specific cell types.[1] Recently, a greater attention has been given to the development of so-called 4D biomaterials – smart biomaterials that can reversibly or irreversibly change shape, size, texture, or composition through time and in response to internal programs and/or external stimuli (e.g., temperature, pH, current, osmotic pressure, light).[2] Although there has been some debate around the principles defining which technologies can or cannot be considered 4D, it is clear that the self-change over time needs to be programmed *a priori* and not be a time-dependent, naturally-occurring remodeling.[3] Some of these biomaterials are designed as synthetic cell scaffolds that change their intrinsic properties upon a specific stimulation,[4] usually aiming at improving cell behavior and/or tissue function post-implantation. Other 4D approaches focus instead on exploring living cells as the force generators to drive changes in their supporting scaffolds.[5] In particular, sheets of contractile cardiomyocytes[6] or skeletal muscle cells[7] have been used as bio-actuators to promote the rapid and dynamic shape-change of elastomer frames and produce motion. However, and to our present knowledge, cells have not yet been used as bio-actuators to improve the function of 4D-engineered biological tissue equivalents.

In particular, we were interested in using such bio-actuator systems to produce curved collagen gels that could recreate the shape of the human cornea. This outermost tissue of the eye is comprised of a dense collagen stroma, where shape, composition, and ultra-structural organization all play a closely integrated and crucial role in maintaining the tissue's strength, transparency, and ability to refract light.[8] Previous attempts to recreate this functionally complex tissue have tried to address different challenges by adopting either top-down or bottom-up tissue engineering strategies. For

example, top-down approaches typically combined cells with cornea-shaped matrices fabricated via molding,[9] electrospinning,[10] 3D bio-printing,[11] or mechanical strain[12] to rapidly produce transplantable tissues.[13] However, these tissues have demonstrable limitations in terms of recreating the important ultrastructural and compositional properties of the tissue, such as the lamellar organization of the matrix, the dimension, density, and alignment of collagen fibrils, and the ratio between different ECM components. [14] In contrast, bottom-up approaches have allowed the bio-fabrication of more native-like tissues in terms of shape,[15] ultrastructure, [16] and composition [16a, 16b, 17], but these methods are slower and still unable of producing full-thickness corneas.

In previous studies, we explored potential methods to improve the function of corneal stromal equivalents, namely by modulating the contractile activity of stromal cells incorporated within 3D collagen scaffolds through the addition of a bio-functional peptide amphiphile.[18] Briefly, we created collagen hydrogels combined with a lipopeptide comprising the cell-binding RGDS peptide motif to provide a preferential adhesion cue for human corneal stromal cells. Subsequently, these lipopeptide-collagen composite scaffolds were shown to contract less than their collagen-only counterparts, with the contractile activity of stromal cells inhibited via specific RGDS-integrin interactions.[18] This important finding allowed us to devise a new 4D tissue engineering system, whereby stromal cells can promote tissue self-curvature through the precise spatial distribution of their bio-actuator activity. Specifically, we used the stromal cells-adhesive $C_{16}G_3$RGDS peptide amphiphile (**Figure 1a**)[19] to program the trajectories of cell contraction in well-defined regions of compressed collagen gels and create strain differentials similar to those observed during the morphogenesis of dome-shaped tissues.[20] Interestingly, the resulting tissues not only achieved a cornea-shaped curvature but also presented a more native-like ultrastructure and composition, with self-curved tissues evidencing higher cell and ECM organization and improved bio-function. Overall, this study illustrates the considerable potential impact of bio-functionalization and cell bio-

actuators in 4D tissue engineering, particularly for the production of improved corneal stromal equivalents.

2. Results and Discussion

2.1 Cell-Driven Contraction of Collagen Gels can be Modulated with Peptide Amphiphiles

The ability to use human corneal stromal cells as tunable bio-actuators was tested by evaluating the impact of cell density and medium composition on collagen gel contraction. Specifically, stromal cells were encapsulated uniformly within compressed collagen gels either at low (LCD) or high cell density (HCD) (0.9 or 1.8 × 10^5 cells per mL of collagen solution, respectively) and cultured for 7 days in the absence (SFM) and presence of serum (+FBS). Results showed a significant ($p < 0.0001$) and time-dependent decrease in gel size for all conditions due to cell-driven contraction (**Figure 1b**). The highest gel contraction was observed for HCD and +FBS culture conditions. The presence of serum in particular drastically contributed to gel contraction, with HCD and LCD gels in +FBS medium at day 7 contracting to 12±3 and 23±6% of their initial size, respectively. This corresponded to a significant ($p < 0.001$) 2.3- and 1.8-fold increase in contraction over HDC and LCD gels in SFM (50±2 and 67±3% of initial size, respectively) (**Figure 1b**). These differences were expected, as serum has been shown to activate stromal cells toward a contractile, myofibroblast-like phenotype.[21] In contrast, cell density showed to have a more limited (albeit still significant) impact on gel contraction, with HDL in +FBS and SFM inducing a significant 1.1- and 1.5-fold increase in gel contraction compared to their LCD counterparts ($p = 0.026$ and 0.013, respectively) (**Figure 1b**).

Likewise, the ability to modulate stromal cells-driven gel contraction using the self-assembled $C_{16}G_3$RGDS peptide amphiphile (PA) within gels was evaluated. Specifically, the inhibitory effect of this PA in gel contraction was investigated by culturing cell-encapsulated, compressed PA/collagen gels for 7 days in +FBS and SFM conditions (**Figure 1c**). Gels without PA or without cells were used as positive and negative contraction controls, respectively. Gels containing PA (+PA) showed significantly lower contraction compared with gels without it (-PA), both in +FBS (up to day 5, $p = 0.042$) and SFM conditions (from day 2 onwards, $p = 0.039$) (**Figure 1d**).

Furthermore, +PA gels showed no significant reduction in size compared to gels without cells (no cell control) both in +FBS (up to day 3) and SFM conditions (during the entire culture period) (**Figure 1d**). The ability of PA to inhibit gel contraction was similarly observed in previous studies using the Fmoc-RGD functionalizing molecule,[18] then attributed to the preferential binding of cells to the adhesion peptide. Together, these results demonstrate that stromal cells have the ability to contract the gels in a time-dependent manner, and that this bio-actuator activity can be modulated by different cell density, medium conditions, and collagen gel functionalization using a PA.

2.2 Defined PA Localization within Composite Gels Allows Tissue Self-Curvature

Having demonstrated that stromal cells could be controlled to function as bio-actuators, we designed and produced composite gels, with PA limited to either the center (inner-PA) or periphery (outer-PA) of the gels (**Figure 2a**). We hypothesized that the presence of PA would decrease the rate of gel contraction within a limited area of the gels, and consequently create a contraction differential between the gels' center and periphery that would result in tissue shape change. Composite gels 120-150 µm thick were thus cultured for up to 7 days either in +FBS or SFM. Interestingly, both inner-PA and outer-PA composite gels showed a gradual shape change when in +FBS condition (**Figure 2b**), visibly increasing their curvature over the course of the culture period (**Video 1**; **Video 2**). The direction of this curvature was independent of PA localization, with both inner-PA and outer-PA equally contracting into convex and concave cornea-shaped tissues (**Figure 2c**). This effect further indicated that gel curvature was not gravity-driven, but the result of a change in the intrinsic structure of the gels via actuation by the highly viable stromal cells (**Figure 2d**). Curvature directionality may depend on stochastic distribution of stromal cells, with higher cell density on the top or the bottom of the gels leading to concave or convex curvature, respectively. Self-curved composite gels also displayed good structural integrity over the time in culture, with the presence of PA having no apparent effect on gel stability. Furthermore, these gels were able to retain their curved shape even after extensive handling (**Video 3**). Moreover, self-curvature did not

visibly reduce gel transparency compared to that of planar gels (**Figure S1**). After 5 days in +FBS conditions, gels assumed a more pronounced ellipsoid shape, with curvature angles of 20 ± 1° (**Figure 2e**), and a ratio between diameter/curvature radius similar to that of the native cornea (i.e., approximately 1.4).[22] Beyond the fifth day in +FBS culture, gels continued to contract and lost their distinct cornea-like shape whilst maintaining high cell viability, both in the center and periphery of the gels (**Figure 2d**). In contrast, gels in SFM maintained their initial planar shape (**Figure 2e**) despite their mild contraction and the high viability of their encapsulated cells (**Figure 2d**).

2.3 The Contractile Phenotype of Stromal Cells in Self-Curved Composite Gels

The effect of the different culture conditions on the contractile phenotype of encapsulated stromal cells was evaluated by in-cell Western blotting. This approach allowed us to compare the total amount of protein and its relative distribution across the constructs simultaneously. Firstly, the expression of the α-smooth muscle actin (αSMA) contraction marker was quantified in self-curved and planar gels after 5 days in +FBS and SFM, respectively, by near-infrared fluorescence analysis. Protein expression was also distinguished between the regions of tissues with (+PA) or without PA (-PA). Ostensibly, self-curved gels showed higher αSMA expression compared to planar gels (**Figure 3a**). This was an expected outcome, since stromal cells in +FBS conditions are known to acquire a contractile phenotype dependent on αSMA stress fibers,[23] whereas SFM keeps cells in a quiescent, non-contractile state by preventing the formation of such fibers.[24] However, no significant differences in αSMA expression were shown between +PA and -PA areas of composite gels (**Figure 3a**). This result was surprising in view of the PA's strong inhibitory effect on gel contraction previously observed (**Figure 1**), and suggested that its modulating activity was not exerted via direct regulation of cell phenotype. This notion was supported by the levels of αVβ5 integrin and keratocan (markers of activated[25] and quiescent stromal cells,[26] respectively), both of which were not altered by the presence of PA, either in +FBS or SFM conditions (**Figure 3b**).

Instead, the PA probably acted by providing a ligand within the structural collagen matrix to which cells preferentially adhered (*i.e*. a scaffold-within-a-scaffold).[18] As collagen fibrils forming the main structural component of our composite gels were not chemically cross-linked to the PA, this allowed PA-bound cells to freely contract while exerting a reduced actuation on the overall shape and density of the tissue. Taken together, these results further support the concept of gel self-curvature being induced by the localized contractile activity of myofibroblast-like stromal cells, with PA preventing, in part, the action of such contractile cells on the collagen gel matrix.

2.4 Self-Curvature Induces Cell and ECM Reorganization

Confocal microscopy was used to evaluate the organization of stromal cells encapsulated in inner-PA and outer-PA composite gels cultured either in +FBS or SFM (**Figure 4**). Specifically, composite gels were collected every day, up to day 5 of culture (the time necessary to achieve a homogeneous curvature in +FBS conditions), and then fixed, and incubated with phalloidin (to image the actin cytoskeleton) and anti-collagen I antibody. Both types of self-curved gels (inner-PA and outer-PA) showed increasing stromal cells' organization throughout the culture period, with cells gradually assuming higher degrees of alignment over time (**Figure 4**; **Figure S2**). Specifically, cells encapsulated within self-curved gels displayed a more uniform orientation after 5 days in culture, with orthogonal-like alignment in both their center and periphery regions (**Figure 4**, self-curved gels). In contrast, cell orientation within planar gels (cultured in SFM) was mostly random (**Figure 4**, planar gels). Interestingly, the stromal cells within 200-300 μm of the outer edges of the gels showed a uniform circumferential alignment independent of the culture condition (**Figure S2**). This alignment was likely related to a boundary effect initiated by the compression method, as suggested by the similar edge-parallel cell orientation immediately after compression of square-shaped collagen gels (**Figure S3**). Together, these results indicated that self-curved 4D tissues promoted a more organized cell alignment and distribution, starting after the first day in +FBS and progressing throughout the period in culture. This suggested that stromal cells' orientation changed

in response to the cell-driven, PA-modulated tissue self-curvature and not vice versa, *i.e.* bio-actuation induced cell reorganization and alignment along with gel contraction into a cornea-like shape. This notion was supported by the cell-orientation effects observed in corneal stroma models subjected to equibiaxial strain.[12] But most importantly, the cells orientation within self-curved 4D tissues, and particularly their orthogonal alignment in the center, had a striking similarity to that of cells in the native corneal stroma.[27]

The orientation of the collagen fibrils comprising the various gels was analyzed using atomic force microscopy (AFM). Specifically, the surface topography of self-curved (+FBS) inner-PA and outer-PA gels was evaluated and compared with that of planar (SFM) tissues. Similarly to what was observed for encapsulated stromal cells, collagen fibrils from self-curved gels were shown to acquire a more regular orientation over time (**Figure 5a**, day 1 *versus* day 5), with highly aligned, orthogonal-oriented fibrils forming a relatively smooth surface topography in both center and periphery regions after 5 days in +FBS culture (**Figure 5b**). Conversely, planar gels showed to maintain a mostly random-oriented collagen fibril distribution (**Figure 5a**) and a rougher topography (**Figure 5b**) similar to that of gels without encapsulated cells (**Figure S4**). These differences clearly indicated that cell-driven contraction was accompanied by an ultrastructural rearrangement (remodeling) within the 3D gels. Furthermore, the topographical smoothing of self-curved gels was significantly higher ($p < 0.05$) in the areas without PA (**Figure 5b**), providing further evidence of a PA-modulated bio-actuation differential. The resulting strain differential therefore corresponded to well-defined, localized distortion of the gels' 3D matrix (i.e., increased fibril density and anisotropy), which in turn promoted the change from a planar to a regularly-curved, synclastic shape similar to that achieved via a tension-actuated tile-and-pin design[28] or mechanical compaction.[20] This stands in clear contrast to 3D gels with uniform or randomly dispersed bio-actuation (e.g. gels without PA or with uneven cell distribution), where stochastic deformation paths derived from multiple matrix contraction and rearrangement sites resulted in multiple folds (**Figure S5**). These results supported the notion that contracting stromal cells acted

on the matrix components of the gels (presumably via cell-collagen interactions),[29] and that the constant and progressive biomechanical tension exerted was instrumental for collagen fibril stretching,[30] ECM reorganization[31] and tissue self-curvature over time. In contrast, the lack of contracting stromal cells in SFM conditions allowed collagen fibrils to remain randomly orientated, relaxed, and to maintain a planar gel matrix.

2.5 Self-Curvature Modulates the Mechanical Properties of Composite Gels

The mechanical properties of the different constructs were evaluated by force-distance atomic force microscopy, probing distinct areas of the gels. A consistent increase in elastic modulus over time in culture (*i.e.* from day 1 to day 4) was observed in both the center and periphery of inner-PA and outer-PA gels in +FBS conditions (**Figure 6a**), with self-curved gels showing an overall higher stiffness compared to their correspondent planar tissues (SFM) (**Figure 6b**). The higher elastic modulus of gels in the presence of serum was expected, as the activation of stromal cells (and consequently their function as bio-actuators) was the force driving gel contraction (**Figure 1**) and increasing collagen fibril organization (**Figure 5**). Moreover, increased gel stiffness corresponded to lower gel hydration (**Figure S6**). The correlation between increased stiffness and higher contraction/increased matrix organization/reduced hydration is well-documented in collagen-based hydrogels.[32] Interestingly, in +FBS conditions the regions of the gels containing PA (periphery and center for outer-PA and inner-PA, respectively) were significantly softer compared to their counterparts without PA (**Figure 6**, red *versus* black dots). This lower stiffness likewise corresponded to higher gel hydration (**Figure S6**). The impact of PA on the mechanical properties of gels was also observed in composite gels cultured in SFM, but in a much lesser degree (**Figure 6b**). This difference suggested that the PA did not influence the gel stiffness by directly affecting the collagen cross-linking. This notion is supported by the similar mechanical properties between the different regions of gels at day 1 (**Figure 6b**), as well as by the slightly higher hydration of PA-containing regions of the gels (**Figure S6**).

2.6 Effects of Self-Curvature on Corneal Epithelial Cell Growth and Phenotype

The diverse mechanical properties between center and periphery of self-curved composite gels (softer in +PA and stiffer in -PA regions) led us to investigate how these features impacted the growth of human limbal epithelial stem cells. Previous studies have shown that differences in tissue topography and/or compliance can regulate the phenotype of these cells, with more organized, stiffer collagen-based substrates promoting epithelial cells differentiation,[15-16] probably though mechanotransduction signaling pathways.[33] Since the human corneal epithelium requires the support of a well-ordered native stroma in order to maintain its homeostasis,[34] our experiment aimed at demonstrating the suitability of self-curved gels to serve as substrate for the adhesion, growth, and differentiation of the epithelial cells. To this purpose, these cells were seeded onto the periphery of self-curved inner-PA or outer-PA gels and grown on the gels' convex side for 10 days in a liquid environment (**Figure 7a**). Results showed that the epithelial cells were able to attach, migrate, and proliferate across the entire surface of the gels (**Figure 7a**). Subsequently, the effects of the different mechanical properties of their substrate were evaluated through the expression analysis of Δp63 (stem/progenitor cell marker),[35] CK3 (differentiation marker),[36] and YAP, a transcription factor whose nuclear localization has been associated with cell differentiation via mechanosensing.[37] Results showed that epithelial cells on the periphery of inner-PA gels (more organized, stiffer matrix) expressed significantly reduced levels of the stem/progenitor cell marker Δp63 ($p = 0.0012$) compared to cells growing in the center (**Figure 7b**). In addition, cells on the periphery showed YAP predominantly located in the nucleus ($p = 0.009$; **Figure 7b**), a known epithelial cell response to stiff substrates.[33a] This was reversed in cells grown on the center region of inner-PA gels (**Figure 8b**), with the significantly lower nuclear YAP levels ($p = 0.0015$) indicating a change in cell mechanosensing due to higher compliance of the substrate (**Figure 6a**). This change was also accompanied by a significantly lower expression of the differentiation marker CK3 ($p = 0.0001$) in epithelial cells grown on the center of inner-PA gels (**Figure 7b**), a decrease

previously shown to be associated with lower substrate stiffness.[33b] Consistently, epithelial cells grown on outer-PA gels showed the reverse expression pattern (**Figure 7c**), with cells on the center (stiffer matrix) expressing significantly lower levels of Δp63 and cytoplasmic YAP (p = 0.003 and 0.0001, respectively) as well as higher levels of nuclear YAP and CK3 (p = 0.022 and 0.011, respectively) compared to those on the periphery region (**Figure 7c**). Together, these results demonstrated that the PA can locally modulate stromal cells adhesion and their function as bio-actuators, to subsequently produce self-curving tissues with specific and localized structural (**Figure 5**), mechanical (**Figure 6**), and biological properties (**Figure 7)**. Such self-curved gels provided a suitable surface for the attachment and growth of epithelial cells, with outer-PA gels allowing cells to remain undifferentiated in their (softer) periphery while becoming more differentiated their (stiffer) center. This is important, as such biomechanical and bio-functional properties reproduced those of the native tissue, with undifferentiated corneal limbal epithelial stem cells located in the softer limbus and the differentiated epithelium spanning the stiffer center of the anterior cornea.[38]

3. Conclusion

This study demonstrated the possibility to create shape-changing tissues by incorporating bioactive PA nanostructures to modulate cell-driven contraction within their matrix. By creating a differential in bio-actuation between the center and the periphery of the gels while still allowing their ultrastructural remodeling, the incorporated PA promoted the formation of a regularly curved, cornea-like, synclastic shape. Such self-curved tissues thus represented a new and improved model of the human corneal stroma, combining both top-down (*i.e.*, the fabrication of cell-populated gels) and bottom-up tissue engineering approaches (*i.e.*, the cell-driven remodeling of the scaffolds). In this context, these constructs can be considered as potential alternatives of corneal stroma tissue for transplantation. For instance, the concept of self-curving design could easily be integrated into current additive manufacturing techniques such as 3D bio-printing,[39] for scaled-up, GMP-

compliant production supplementing recent advances in the corneal bio-printing field.[11] Such integration would also allow automation, as well as a higher degree of consistency and precision in the spatial localization of the different cellular and matrix components of the composite gels.[40] Ultimately, these cornea-shaped tissues displayed better cell and ECM organization compared to their planar counterparts. The influence of the bioactive PA was also extended to the tissues' mechanical properties, which in turn allowed the creation of delimited biomechanical niches on their surface as well as the modulation of growth and differentiation of corneal limbal epithelial stem cells. Specifically, the stem cell-like phenotype of the epithelial cells was better supported by tissue regions containing PA, probably due to their lower elastic modulus. In contrast, tissue regions without PA and subjected to increased cell actuation and contraction provided a stiffer matrix that promoted epithelial differentiation. The ability to use PAs to modulate the shape and stiffness of collagen-based biomaterials via the control of cell actuators is a particularly useful tool in 4D tissue engineering, and can thus be translated into a broad range of applications. For example, PAs could be used to rationally design more complex composite materials where structural, biomechanical, and bio-functional properties can evolve towards emulation of a specific native tissue. As such, 4D tissue equivalents not only have the potential to revolutionize tissue engineering and regenerative medicine strategies, but also can contribute to a more fundamental understanding of the mechanisms underlying tissue and organ morphogenesis.

4. Experimental Section

Human Corneal Cells Isolation and Culture: Stromal and epithelial cells were isolated from cadaverous human corneal tissue (donors' age between 40 and 78; average ± S.D. = 59 ± 11 years, male-female donor ratio of 2:3, with no prior history of corneal diseases or ocular trauma). All human corneas were collected from NHS Blood and Transplant (NHSBT) via a service level agreement with Newcastle-upon-Tyne Hospitals NHS Foundation Trust, UK. All donors approved the use in research of their corneal tissues, in full accordance with the regional ethics committee approval and research agreement. Briefly, each corneal ring was gently scraped to remove the endothelium, cut radially in 6 pieces of equivalent size, individually placed in 6-well plate (Greiner Bio-One, Austria) with the epithelium-side facing the bottom of the well and cultured for 10 days in 4 mL of CnT-7 medium (CellNTec, Switzerland) at 37°C, in humidified and 5% CO_2 cell culture incubator conditions. Subsequently, the corneal pieces were removed while the epithelial cells previously shed by the tissues during culture were enzyme-dissociated from the plate surface with StemPro Accutase (Thermo Scientific, MA, USA) for 10 min and passaged for expansion in tissue culture flasks (Greiner Bio-One) with CnT-7 medium. Media were replaced every 2 days following a gentle wash with phosphate buffered saline (PBS) (Thermo-Scientific) and epithelial cells were used for subsequent experiments up to the second passage. Corneal pieces were further used to extract stromal cells. Briefly, corneal tissues were minced using a scalpel, transferred to DMEM/F12 medium (Thermo Scientific) supplemented with 5% fetal bovine serum (FBS) (BioSera, France), 2 g L^{-1} (450 units mL^{-1}) collagenase type-1 (Thermo Scientific) and incubated at 37°C in a humidified, 5% CO_2 incubator under continuous rotation for 5 h, followed by incubation with 0.25% trypsin-EDTA (Thermo Scientific) for 10 min. The isolated stromal cells were collected and plated onto tissue culture flasks and maintained using serum-containing medium (+FBS) comprising DMEM/F12 medium supplemented with 5% FBS and 1% penicillin/streptomycin (Thermo Scientific), with medium changed every 2-3 days, and cultures maintained until reaching 70-80% confluence. Cells were then serum-starved for three days in serum-free medium (SFM)

comprising DMEM/F12 with 1 x 10^{-3} M ascorbic acid (Sigma Aldrich, MO, USA), 1× ITS (Sigma Aldrich), and 1% penicillin/streptomycin to induce quiescence. Cells were detached using TrypLE™ express enzyme (Thermo Scientific) and encapsulated in collagen gels. Each experiment was performed thrice using stromal cells up to passage 5, from three different donors.

Preparation of Peptide Amphiphiles: The $C_{16}G_3$RGDS peptide amphiphile (PA) was custom-synthesized by CS Bio (Menlo Park, CA, USA) as >95% pure trifluoroacetic acid salts and its molecular weight (842.95 g mol^{-1}) confirmed by electrospray-mass spectrometry.[41] The PA was then weighted and solubilized in SFM at 5 mM and stored at 4°C until added to the collagen gel solution in a 1:10 (vol:vol) ratio.

Preparation of Compressed Collagen Gels: Functionalized constructs were prepared by combining PA with compressed collagen gels in well-delimited areas, either in the center (inner-PA gels) or in the periphery (outer-PA gels). To achieve such precise spatial localization, a two-step process was adopted. Firstly, the central gels were prepared within 15.6 mm Ø wells of 24-well plates (Greiner Bio-One) by mixing 0.9 mL of neutralized collagen solution with 0.1 mL of PA in SFM solution (for inner-PA gels) or SFM alone (for outer-PA gels), with or without human corneal stromal cells. Specifically, rat tail collagen type I (2.05 mg mL^{-1} in 0.6% acetic acid, First Link, UK) was mixed with 10× modified Eagle's minimum essential medium (Thermo Scientific) and sodium hydroxide 1M (Thermo Scientific) to form the neutralized collagen solution, which was then mixed with PA/SFM or SFM with and without cells (1×10^5 serum-starved stromal cells mL^{-1}), in a 7:1:1:1 volume ratio, respectively.[18] The central collagen gel solution was polymerized at 37°C in a humidified 5% CO_2 incubator for 30 min, and then gently removed from the molds, transferred into the center of a 22.1 mm Ø well of 12-well plates (Greiner Bio-One), and then surrounded by an identical collagen mixture (0.9 mL of neutralized collagen solution and 0.1 mL of PA (for outer-PA gels) or SFM (for inner-PA gels). This mixture was then allowed to polymerize to obtain a

composite gel with a seamless core-periphery interface and subsequently transferred in between layers of nylon mesh and compressed at room temperature with a 134 g or 154 g load (for gels with or without cells, respectively) for 5 min in sterile conditions. The resulting composite gels were then transferred to a 6-well plate (Greiner Bio-One) and cultured in +FBS or SFM up to 7 days with media changed every 2-3 days. All experiments were performed in an aseptic Class II cell culture cabinet.

Gel Contraction Assays: The rate of gels' contraction was monitored by digital photography every 24 h, up to day 7 in culture, using a Nikon D90 digital camera (Nikon, Japan). Images were then analyzed using ImageJ v1.46, with three measurements of the gels' diameter to calculate tissue area and evaluate the average gel contraction in the different conditions, expressed as percentage decrease in surface area compared to the initial gel surface area. All experiments were performed three independent times, in triplicate (n = 3).

Live/Dead Double-Staining of Embedded Cells: To assess the viability of the encapsulated cells, the live/dead double staining using calcein-AM (Sigma Aldrich) and propidium iodide (PI; Sigma Aldrich) was performed following 7 days in culture according to the manufacturer's instructions. Briefly, functionalized gels were washed with PBS and incubated in the dark for 30 min at 37°C with PBS supplemented with calcein-AM and PI at 1 µM. The gels were then examined using a Axiovert 1 fluorescence microscope (Zeiss Microscopy, Germany) using the appropriate filter blocks to observe the presence of live (green) and dead (red-stained) cells. Fluorescence images were subsequently analyzed and merged using ImageJ v1.46. All experiments were performed in triplicate (n = 3).

Culture of Epithelial Cells on Compressed Collagen Gels: Functionalized gels at day 5 of culture were mounted onto curved glass lenses (13 mm Ø; contact angle: 45°) in 6-well plates, pinned

down using metal rings (inner Ø: 15 mm; outer Ø: 25 mm), and then were seeded with epithelial cells on their top surface (7.5×10^4 cells per gel). Such cells were then cultured in CnT-7 medium for 10 days to evaluate their growth and phenotype in response to their different gel substrates, and with medium change every 2-3 days.

In-Cell Western Blotting: The expression of protein markers from gel-encapsulated stromal cells was quantified following different culture conditions by near-infrared fluorescence analysis (in-cell Western blotting). Briefly, gels with or without cells cultured for 5 days were fixed with 2% paraformaldehyde (PFA) (Sigma Aldrich), washed twice in PBS, re-washed for 10 min in PBS supplemented with 0.25% Triton X-100 (PBS-T), and then incubated for 1 h with blocking solution (PBS-T with 5% BSA) at room temperature. Subsequently, samples were incubated for 2 h with primary antibodies against αSMA (VPS281, Vector Labs, UK), αVβ5 integrin (ab24694, Abcam, UK) or keratocan (sc-66941, Santa Cruz Biotechnology, CA, USA) diluted 1:1,000 in blocking solution at room temperature. After three washes in PBS-T, samples were then incubated for 1 h at room temperature and with gentle agitation with corresponding anti-mouse or anti-rabbit IRDye 800-conjugated secondary antibodies and CellTag 700 cell marker (LI-COR Biotechnology, UK) diluted 1:25,000 in blocking solution. Subsequently, gel samples were washed thrice in washing buffer and analyzed using the Odyssey CLx near-infrared system (LI-COR Biotechnology). Signals from each specific protein were quantified and normalized for the corresponding cell marker signal using Image J v1.46. Experiments were performed in triplicate ($n = 3$).

Confocal Immunofluorescence Analysis: Confocal microscopy was used to evaluate the arrangement of stromal cells within the various functionalized gels, as well as the phenotype of the epithelial cells grown on their surface. Briefly, gels with encapsulated stromal cells were fixed in 4% PFA for 30 min at different time-points (from day 0 to day 7). After three washes with PBS for 5 min, samples were blocked for 1 h in PBS supplemented with 2% BSA, incubated for 4 h with

rabbit anti-collagen type I primary antibody (ab34710, Abcam) diluted 1:500 in blocking solution, washed thrice with PBS for 5 min, and incubated for 2 h with Texas Red-conjugated goat anti-rabbit IgG antibody (TI-1000, Vector Labs), Alexa Fluor 488-conjugated phalloidin (Thermo Scientific), and DAPI (Thermo Scientific) diluted 1:1,000 in blocking solution. The gels were then washed three times with PBS for 5 min, mounted onto glass slides in glycerol (Sigma Aldrich) and imaged using an A1R confocal laser microscope (Nikon) with constant illumination and capture parameters. In particular, a Galvano scanner was used to acquire 2-5 µm thick *z*-stacks through the entire thickness of the sample using Nikon Plan Apo λ 10× or 20× objectives (NA 0.45 or 0.75, working distance 4 or 1 mm, FOV 1.27×1.27 mm or 0.64×0.64 mm, respectively). Micrographs were then analyzed using the NIS-Elements and ImageJ v1.46 software packages. Immunostaining and imaging of the epithelial cells grown on gels for 10 days was performed as described above, but using anti-CK3 (ab129910, abcam) with anti-CK15 (MA1-90929, Thermo Scientific), or anti-YAP (sc-17141, Santa Cruz Biotechnology) with anti-Δp63 (sc-8431, Santa Cruz Biotechnology) primary antibodies diluted 1:500 in blocking solution. These samples were subsequently incubated with corresponding anti-mouse (TI-2000, FI-2000), anti-rabbit (FI-1000, Vector Labs), and anti-goat (sc-2783, Santa Cruz Biotechnology) secondary antibodies diluted 1:1,000 in blocking solution. Immunofluorescence analysis was performed three independent times, in triplicate ($n = 3$).

Atomic Force Microscopy (AFM): The topographical distribution of collagen fibrils in composite gels was analyzed by atomic force microscopy (AFM) using a Easyscan 2-controlled atomic force microscope (Nanosurf, Switzerland) equipped with ContAI-G soft contact mode cantilevers (BudgetSensors, Bulgaria) with a resonant frequency of 13 kHz and nominal spring constant of 0.2 N/m.

Briefly, gels were fixed in 4% PFA for 30 min at different time-points (from day 0 up to day 7), washed thrice with PBS, dried overnight over a glass slide (Bemis, USA) covered with three layers of parafilm (P7793, Sigma Aldrich) to minimize sample displacement and drift. Surface topography

was analyzed in three separate regions per sample with 512× two-direction lines scanned at 10 μm s^{-1}, at 1 nV, and with P- and I-gains of 1. Topographic data was processed for line wise and tilt correction using the Scanning Probe Image Processor software package (Image Metrology A/S). Data was analyzed using the OrientationJ plugin from ImageJ v1.46 for measuring dimensions and distribution of specimens. Moreover, the stiffness of different samples was evaluated from 20 force-distance curves acquired at 2 μm·s^{-1} from different positions across each sample, and using AtomicJ 1.7.3 data analysis software for baseline and hysteresis correction, followed by elastic modulus calculation using the Sneddon sphere model, applicable for soft biological materials. All experiments were performed in triplicate on four individual areas in each sample (n = 3).

Analysis of the Hydration of Self-Curved Tissues: The weight of gels (with or without encapsulated cells) was measured immediately after compression and after culture to find their corresponding initial and final wet weight (W_i and W_f, respectively). For composite inner-PA and outer-PA gels, different samples were used for initial and final measurements, as gels were excised with a scalpel to separate their periphery and center regions, for each region to be weighted independently. The variation in wet weight (ΔW) was then expressed as the ratio $\Delta W = W_f / W_i$ (Equation 1). Subsequently, the percentage of water bound to the different gels was determined by freeze-drying (Christ, Alpha 1-2 LD plus) the gels to sublimate their frozen water from the solid to gas phase under controlled pressure. The dry weight (W_d) of all freeze-dried gels was then measured, and used to calculate the gels' hydration using the formula for Hydration (%) = $(1 - W_d / W_{i,f}) \times 100$ (Equation 2).

Statistical Analysis: Differences between groups were determined using one- or two-way analysis of variance (ANOVA) with Bonferroni's multiple comparison *post hoc* test. Error bars represent the standard deviation of the mean. Significance between groups was established for $p < 0.05$, 0.01, 0.001, and 0.0001.

Supporting Information

Supporting Information is available from the Wiley Online Library or from the author.

Acknowledgements

This work was supported by the Biotechnology and Biological Sciences Research Council (BBSRC-UK), grant reference BB/N021576/1, Engineering and Physical Sciences Research Council (EPSRC-UK), grant reference EP/L020599/1 and the Newcastle University Postgraduate Studentship, award reference PHD/IHG/FT/8410F.

Conflict of Interest

The authors declare no conflict of interest.

References

[1] L. G. Griffith, G. Naughton, *Science* **2002**, 295, 1009.

[2] a) T. van Manen, S. Janbaz, A. A. Zadpoor, *Mater Today* **2018**, 21, 144; b) Q. Zhao, H. J. Qi, T. Xie, *Progress in Polymer Science* **2015**, 49-50, 79.

[3] J. An, C. K. Chua, V. Mironov, *Int J Bioprinting* **2016**, 2, 3.

[4] a) I. Apsite, G. Stoychev, W. Z. Zhang, D. Jehnichen, J. Xie, L. Ionov, *Biomacromolecules* **2017**, 18, 3178; b) V. Stroganov, J. Pant, G. Stoychev, A. Janke, D. Jehnichen, A. Fery, H. Handa, L. Ionov, *Adv Funct Mater* **2018**, 28.

[5] a) P. Q. Nguyen, N. M. D. Courchesne, A. Duraj-Thatte, P. Praveschotinunt, N. S. Joshi, *Adv Mater* **2018**, 30; b) L. Ricotti, B. Trimmer, A. W. Feinberg, R. Raman, K. K. Parker, R. Bashir, M. Sitti, S. Martel, P. Dario, A. Menciassi, *Sci Robot* **2017**, 2.

[6] S. J. Park, M. Gazzola, K. S. Park, S. Park, V. Di Santo, E. L. Blevins, J. U. Lind, P. H. Campbell, S. Dauth, A. K. Capulli, F. S. Pasqualini, S. Ahn, A. Cho, H. Y. Yuan, B. M. Maoz, R. Vijaykumar, J. W. Choi, K. Deisseroth, G. V. Lauder, L. Mahadevan, K. K. Parker, *Science* **2016**, 353, 158.

[7] Y. Morimoto, H. Onoe, S. Takeuchi, *Sci Robot* **2018**, 3.

[8] a) J. V. Jester, T. Moller-Pedersen, J. Huang, C. M. Sax, W. T. Kays, H. D. Cavangh, W. M. Petroll, J. Piatigorsky, *Journal of cell science* **1999**, 112 (Pt 5), 613; b) O. Kostyuk, O. Nalovina, T. M. Mubard, J. W. Regini, K. M. Meek, A. J. Quantock, G. F. Elliott, S. A. Hodson, *The Journal of physiology* **2002**, 543, 633; c) K. M. Meek, D. W. Leonard, C. J. Connon, S. Dennis, S. Khan, *Eye* **2003**, 17, 927; d) C. Boote, S. Dennis, Y. Huang, A. J. Quantock, K. M. Meek, *Journal of structural biology* **2005**, 149, 1; e) S. A. Klein, R. B. Mandell, *Investigative ophthalmology & visual science* **1995**, 36, 2096.

[9] F. Li, D. Carlsson, C. Lohmann, E. Suuronen, S. Vascotto, K. Kobuch, H. Sheardown, R. Munger, M. Nakamura, M. Griffith, *Proc Natl Acad Sci U S A* **2003**, 100, 15346.

[10] J. I. Kim, J. Y. Kim, C. H. Park, *Sci Rep* **2018**, 8, 3424.

[11] A. Isaacson, S. Swioklo, C. J. Connon, *Experimental eye research* **2018**, 173, 188.

[12] W. Zhang, J. Chen, L. J. Backman, A. D. Malm, P. Danielson, *Adv Healthc Mater* **2017**, 6.

[13] a) P. Fagerholm, N. S. Lagali, J. A. Ong, K. Merrett, W. B. Jackson, J. W. Polarek, E. J. Suuronen, Y. Liu, I. Brunette, M. Griffith, *Biomaterials* **2014**, 35, 2420; b) H. J. Levis, J. Menzel-Severing, R. A. Drake, J. T. Daniels, *Current eye research* **2013**, 38, 41.

[14] R. M. Gouveia, C. J. Connon, in *Biomaterials and Regenerative Medicine in Ophthalmology (Second Edition)*, DOI: https://doi.org/10.1016/B978-0-08-100147-9.00007-9 (Eds: T. V. Chirila, D. G. Harkin), Woodhead Publishing **2016**, p. 151.

[15] R. M. Gouveia, E. Koudouna, J. Jester, F. Figueiredo, C. J. Connon, *Advanced Biosystems* **2017**.

[16] a) R. M. Gouveia, E. Gonzalez-Andrades, J. C. Cardona, C. Gonzalez-Gallardo, A. M. Ionescu, I. Garzon, M. Alaminos, M. Gonzalez-Andrades, C. J. Connon, *Biomaterials* **2017**, 121, 205; b) R. M. Gouveia, V. Castelletto, I. W. Hamley, C. J. Connon, *Tissue Eng Pt A* **2015**, 21, 1772; c) F. N. Syed-Picard, Y. Du, A. J. Hertsenberg, R. Palchesko, M. L. Funderburgh, A. W. Feinberg, J. L. Funderburgh, *Journal of tissue engineering and regenerative medicine* **2018**, 12, 59.

[17] a) D. Karamichos, M. L. Funderburgh, A. E. Hutcheon, J. D. Zieske, Y. Du, J. Wu, J. L. Funderburgh, *Plos One* **2014**, 9, e86260; b) N. Saeidi, K. P. Karmelek, J. A. Paten, R. Zareian, E. DiMasi, J. W. Ruberti, *Biomaterials* **2012**, 33, 7366.

[18] R. M. Gouveia, R. R. Jones, I. W. Hamley, C. J. Connon, *Biomater Sci-Uk* **2014**, 2, 1222.

[19] R. M. Gouveia, V. Castelletto, S. G. Alcock, I. W. Hamley, C. J. Connon, *J Mater Chem B* **2013**, 1, 6157.

[20] A. J. Hughes, H. Miyazaki, M. C. Coyle, J. Zhang, M. T. Laurie, D. Chu, Z. Vavrusova, R. A. Schneider, O. D. Klein, Z. J. Gartner, *Dev Cell* **2018**, 44, 165.

[21] M. P. Beales, J. L. Funderburgh, J. V. Jester, J. R. Hassell, *Investigative ophthalmology & visual science* **1999**, 40, 1658.

[22] W. A. Douthwaite, *Ophthal Physl Opt* **2003**, 23, 141.

[23] S. E. Wilson, *Experimental eye research* **2012**, 99, 78.

[24] N. Lakshman, A. Kim, W. M. Petroll, *Experimental eye research* **2010**, 90, 350.

[25] M. A. Stepp, *Experimental eye research* **2006**, 83, 3.

[26] E. C. Carlson, C. Y. Liu, T. I. Chikama, Y. Hayashi, C. W. C. Kao, D. E. Birk, J. L. Funderburgh, J. V. Jester, W. W. Y. Kao, *J Biol Chem* **2005**, 280, 25541.

[27] C. Hahnel, S. Somodi, D. G. Weiss, R. F. Guthoff, *Cornea* **2000**, 19, 185.

[28] R. Guseinov, E. Miguel, B. Bickel, *Acm T Graphic* **2017**, 36.

[29] W. M. Petroll, H. D. Cavanagh, J. V. Jester, *Scanning* **2004**, 26, 1.

[30] B. Lee, X. Zhou, K. Riching, K. W. Eliceiri, P. J. Keely, S. A. Guelcher, A. M. Weaver, Y. Jiang, *Plos One* **2014**, 9, e111896.

[31] a) W. R. Legant, J. S. Miller, B. L. Blakely, D. M. Cohen, G. M. Genin, C. S. Chen, *Nat Methods* **2010**, 7, 969; b) H. C. Wells, K. H. Sizeland, N. Kirby, A. Hawley, S. Mudie, R. G. Haverkamp, *J Mech Behav Biomed* **2018**, 79, 1.

[32] A. L. Plant, K. Bhadriraju, T. A. Spurlin, J. T. Elliott, *Biochim Biophys Acta* **2009**, 1793, 893.

[33] a) J. W. Foster, R. R. Jones, C. A. Bippes, R. M. Gouveia, C. J. Connon, *Experimental eye research* **2014**, 127, 37; b) R. R. Jones, I. W. Hamley, C. J. Connon, *Stem Cell Res* **2012**, 8, 403.

[34] M. V. Netto, R. R. Mohan, S. Sinha, A. Sharma, W. Dupps, S. E. Wilson, *Experimental eye research* **2006**, 82, 788.

[35] G. Pellegrini, E. Dellambra, O. Golisano, E. Martinelli, I. Fantozzi, S. Bondanza, D. Ponzin, F. McKeon, M. De Luca, *Proc Natl Acad Sci U S A* **2001**, 98, 3156.

[36] A. Schermer, S. Galvin, T. T. Sun, *The Journal of cell biology* **1986**, 103, 49.

[37] S. Dupont, L. Morsut, M. Aragona, E. Enzo, S. Giulitti, M. Cordenonsi, F. Zanconato, J. Le Digabel, M. Forcato, S. Bicciato, N. Elvassore, S. Piccolo, *Nature* **2011**, 474, 179.

[38] P. Eberwein, J. Nohava, G. Schlunch, M. Swain, *Key Engineering Materials* **2014**, 606, 117.

[39] D. Choudhury, S. Anand, M. W. Naing, *Int J Bioprinting* **2018**, 4.

[40] H. J. Lee, Y. W. Koo, M. Yeo, S. H. Kim, G. H. Kim, *Int J Bioprinting* **2017**, 3, 27.

[41] V. Castelletto, R. M. Gouveia, C. J. Connon, I. W. Hamley, *Faraday Discuss* **2013**, 166, 381.

FIGURES & LEGENDS

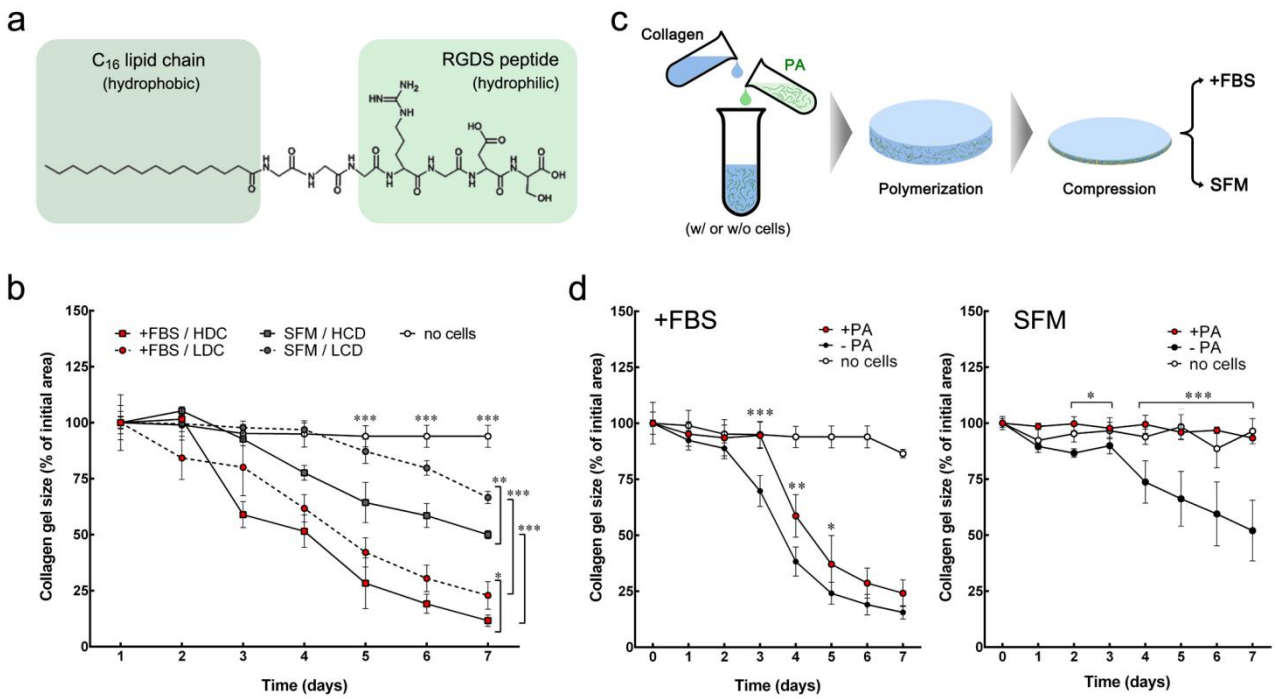

Figure 1: Effect of cell density, culture medium and PAs on gels contraction. (a) Chemical structure of the $C_{16}G_3RGDS$ PA. (b) Contraction of collagen-only gels (as percentage of corresponding initial size) in high (HCD) or low (LCD) cell density conditions, cultured in the presence (+FBS) or absence of serum (SFM). (c) Diagram showing the main steps involved in the preparation and culture of PA-functionalized compressed collagen gels. (d) The inhibitory effect of PA on gel contraction evaluated both in +FBS (left) and SFM conditions (right). Measurements were performed daily, up to 7 days in culture. Differences between average± S.D. area of gels with (+PA) and without PA (-PA) were evaluated for each time point, in three independent experiments (n=3); *, ** and *** corresponded to $p < 0.05$, 0.01 and 0.001, respectively.

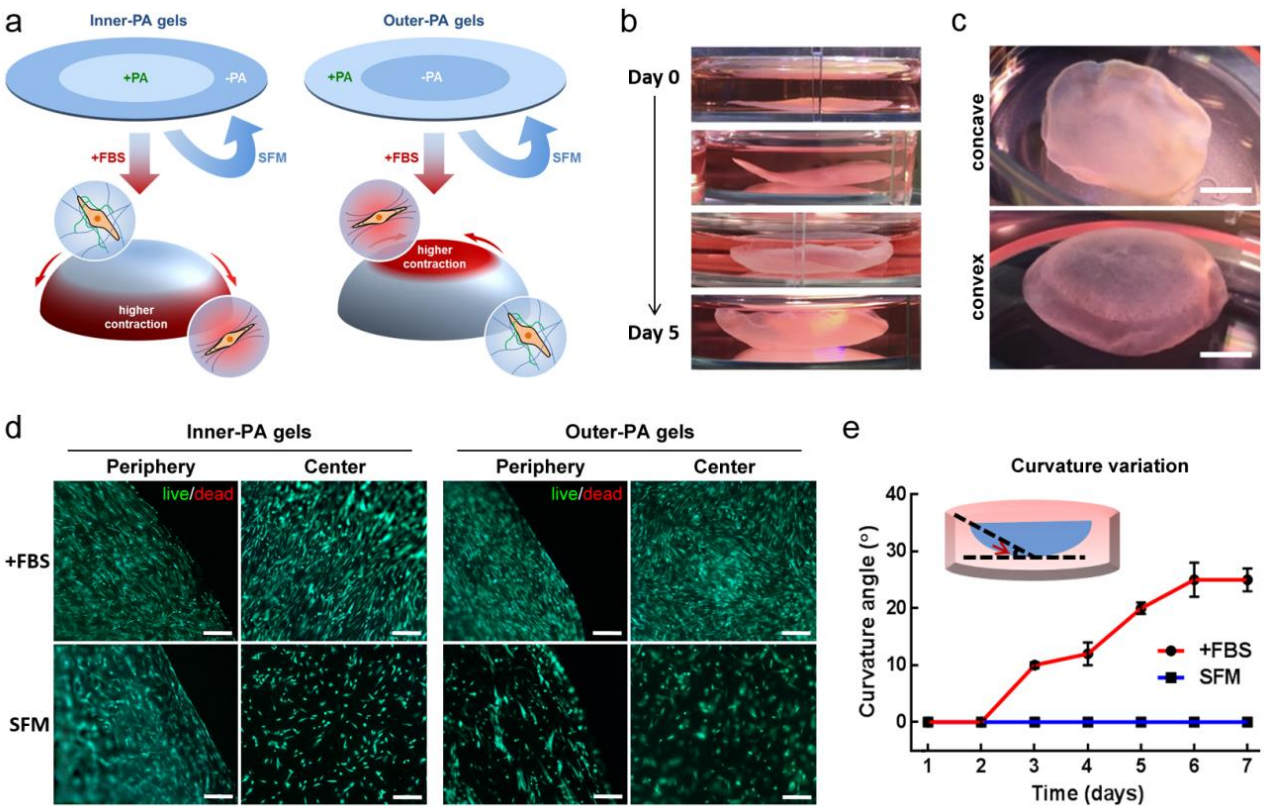

Figure 2: Shape-change and viability of composite gels over time. (a) Schematic of inner-PA and outer-PA gels composition, and the predicted mechanism of differential gel contraction. In +FBS conditions (*red arrows*), cells within the +PA regions of the gels contract less than in the regions without PA, thus driving gel self-curving; gels in SFM conditions (*blue arrows*) do not contract and retain shape. (b) Representative photographs of outer-PA gels self-curving when cultured for 5 days in presence of serum. (c) Representative photographs of self-curved concave and convex inner-PA gels. (d) Representative microphotographs of live (*green*)/dead (*red*)-stained stromal cells within composite gels after 7 days in +FBS and SFM culture conditions, showing a highly viable cell composition. (e) Variation of gels' curvature during a 7 day-culture in +FBS and SFM. Scale bars: (c) 500 µm and (d) 200 µm.

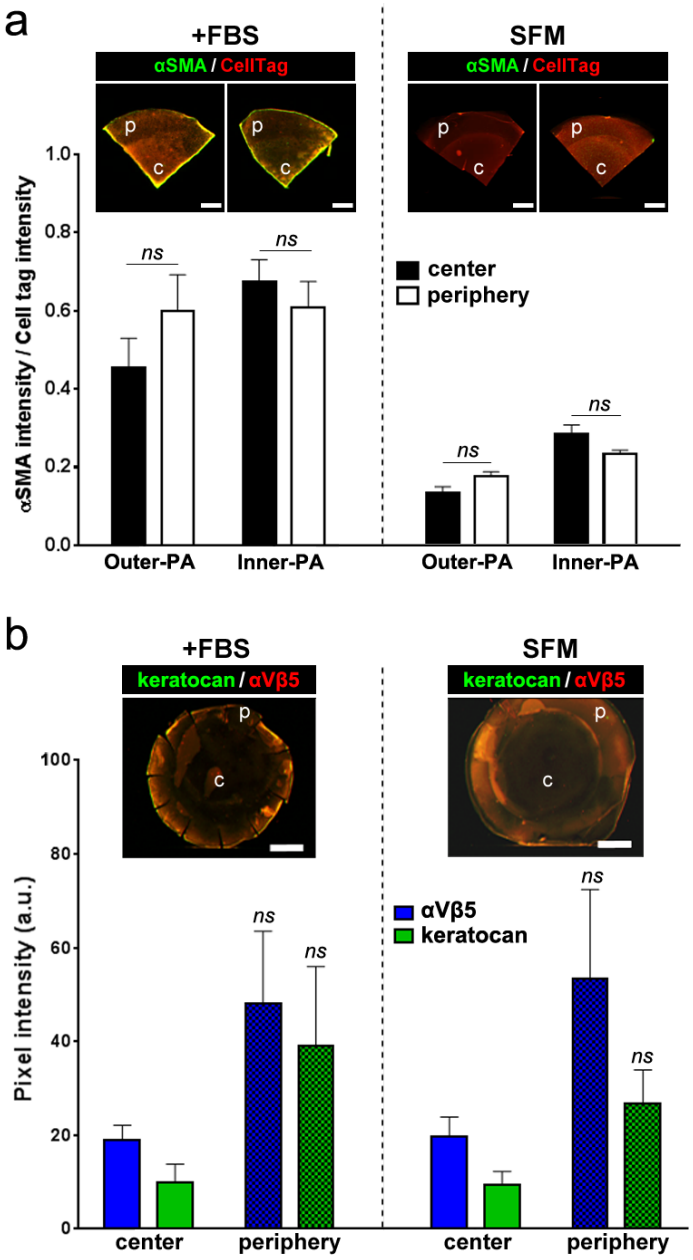

Figure 3: Effect of PAs on the expression of key markers of stromal cells in self-curved and planar constructs. (a) Expression of αSMA (normalized per intensity of the Cell Tag™ marker) by stromal cells encapsulated in the center (*c*) and periphery (*p*) of the gels after 5 days of culture in the presence (+FBS) or absence of serum (SFM). (b) Expression of αVβ5 integrin and keratocan (as arbitrary unit) by stromal cells in outer-PA gels. Representative images are shown for each condition. Scale bars: 500 µm.

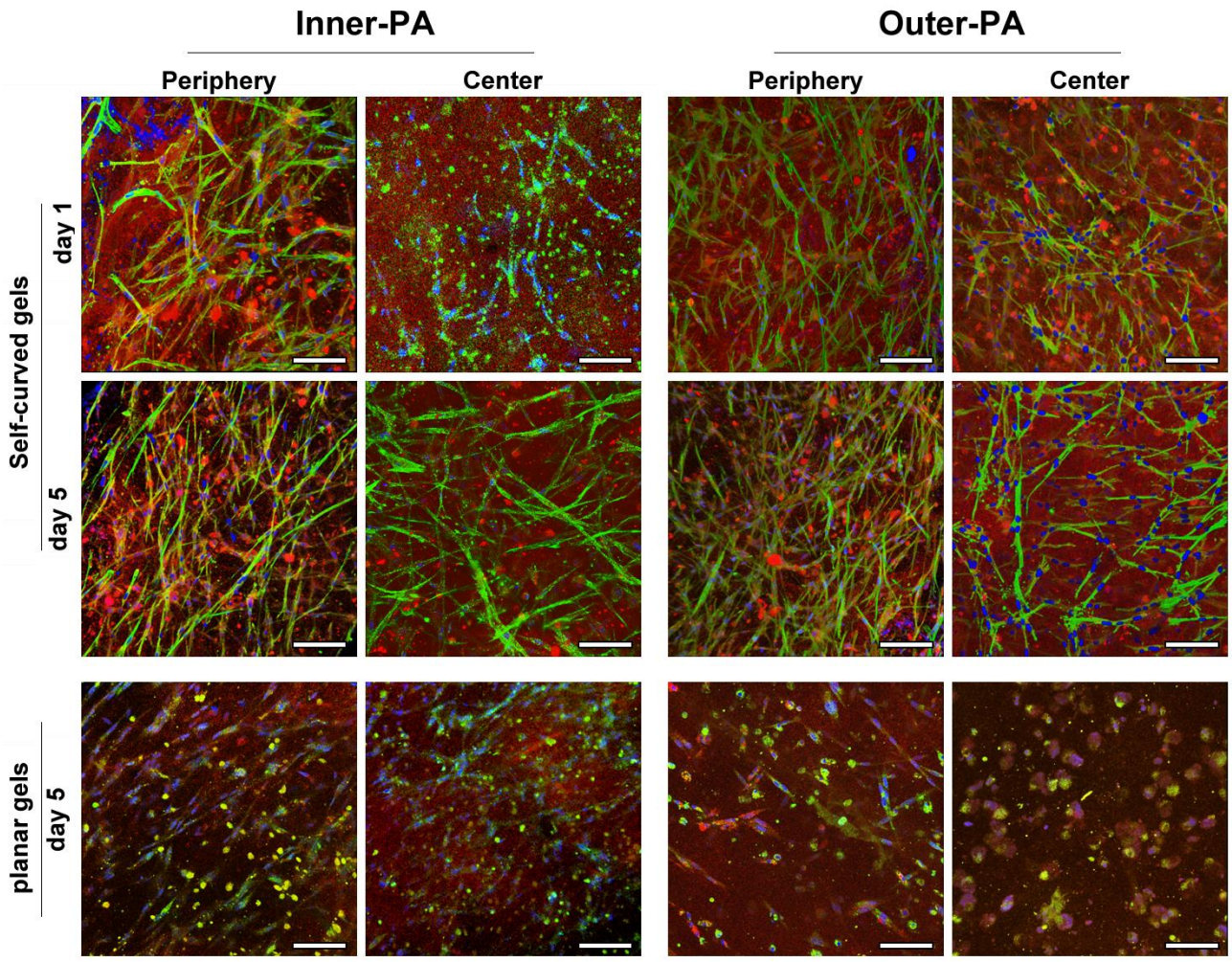

Figure 4: Organization of stromal cells within inner-PA and outer-PA gels. Representative 3D reconstruction of confocal immunofluorescence images of the periphery and center of the gels acquired after 1 and 5 days in +FBS (self-curving gels) or SFM (planar gels). All the gels were stained for collagen I (*red*), F-actin (*green*, phalloidin) and nuclei (*blue*). Scale bars: 100 µm.

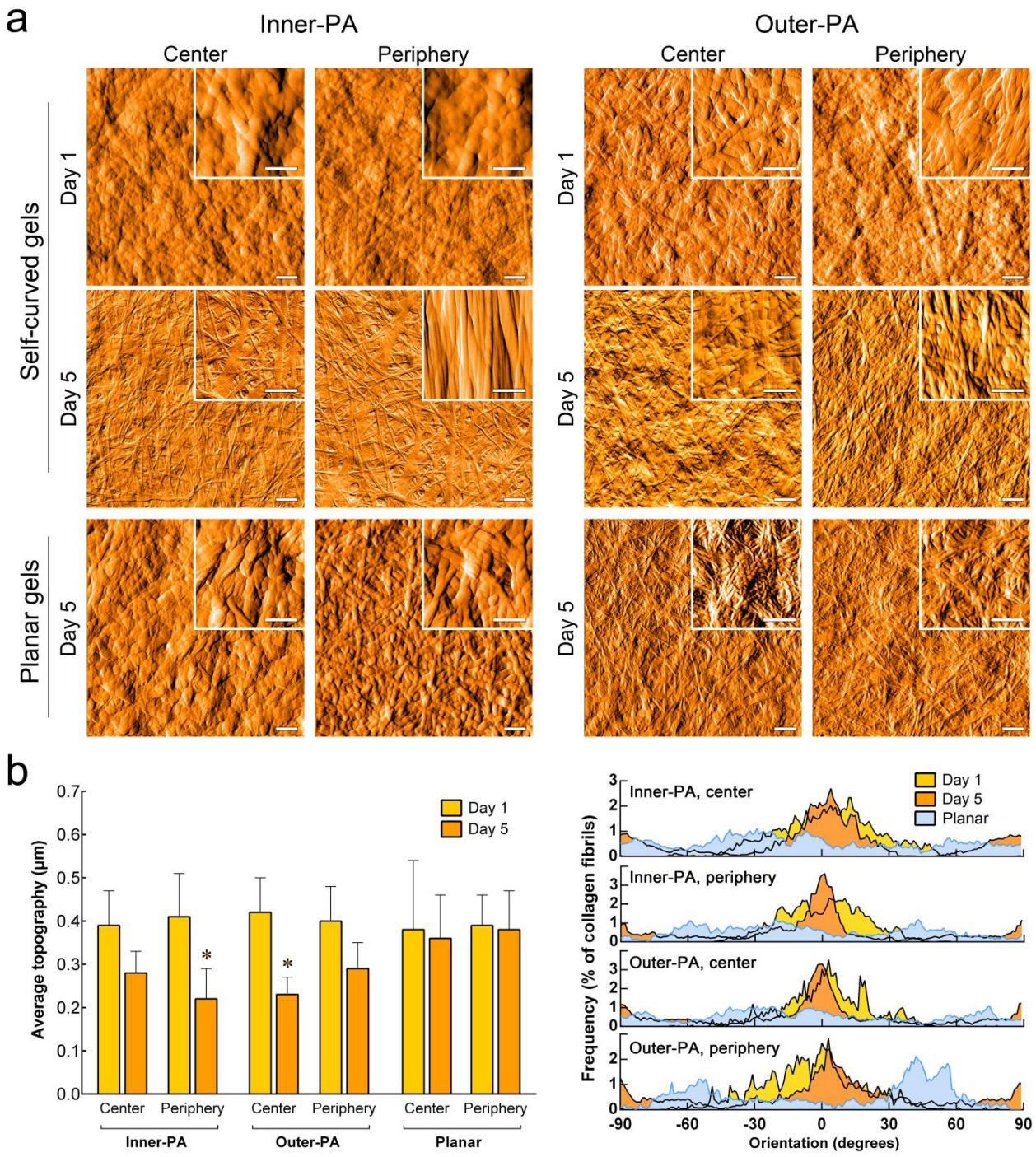

Figure 5: Topography of self-curving gels. (a) Representative atomic force microscopy (AFM) images of inner-PA and outer-PA gels after being cultured for 1 and 5 days in +FBS (self-curved gels) or SFM (planar gels). (b) Gels' topography was quantified in terms of roughness (left) and collagen fibril orientation (right panels), with self-curving gels shown to acquire a more compact, ordered structure (narrowing of peaks) over time irrespective of the PA being loaded at periphery or center of the gels. Scale bars: 1 μm, 0.2 μm (insets).

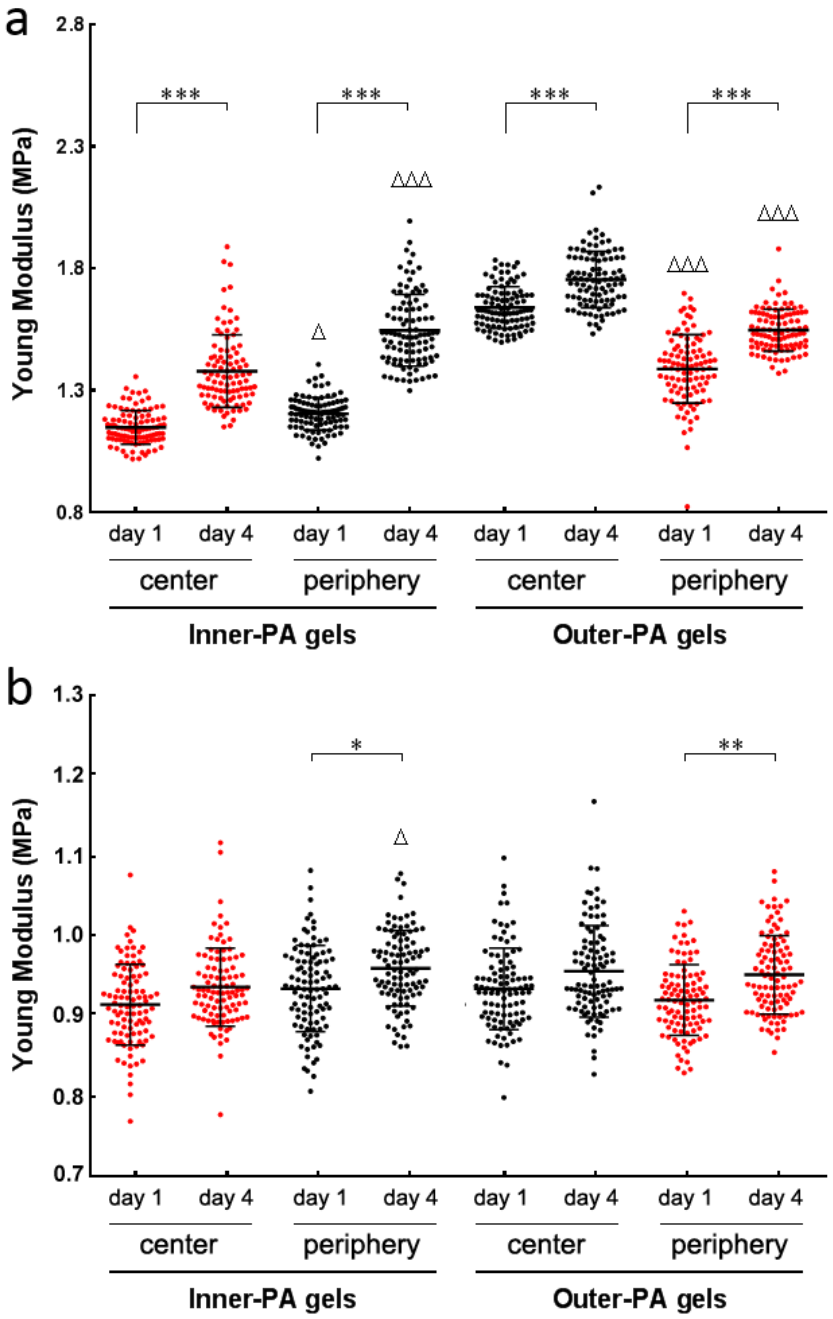

Figure 6: Mechanical properties of inner-PA and outer-PA gels. Graphs showing the stiffness of outer-PA and inner-PA gels after 4 days in culture either in +FBS (a) or in SFM condition (b) are reported. The colored points (*red*) correspond to regions of the gel containing PA. Mean ± S.D., n = 3 for all experiments; * and *** referred to statistically significant differences between the same regions at different time points (effect of time) and corresponded to $p < 0.05$ and 0.001, respectively. $^{\Delta}$ and $^{\Delta\Delta\Delta}$ referred to statistically significant differences between different regions of the same gel for the same time point (effect of PA) and corresponded to $p < 0.05$ and 0.001, respectively.

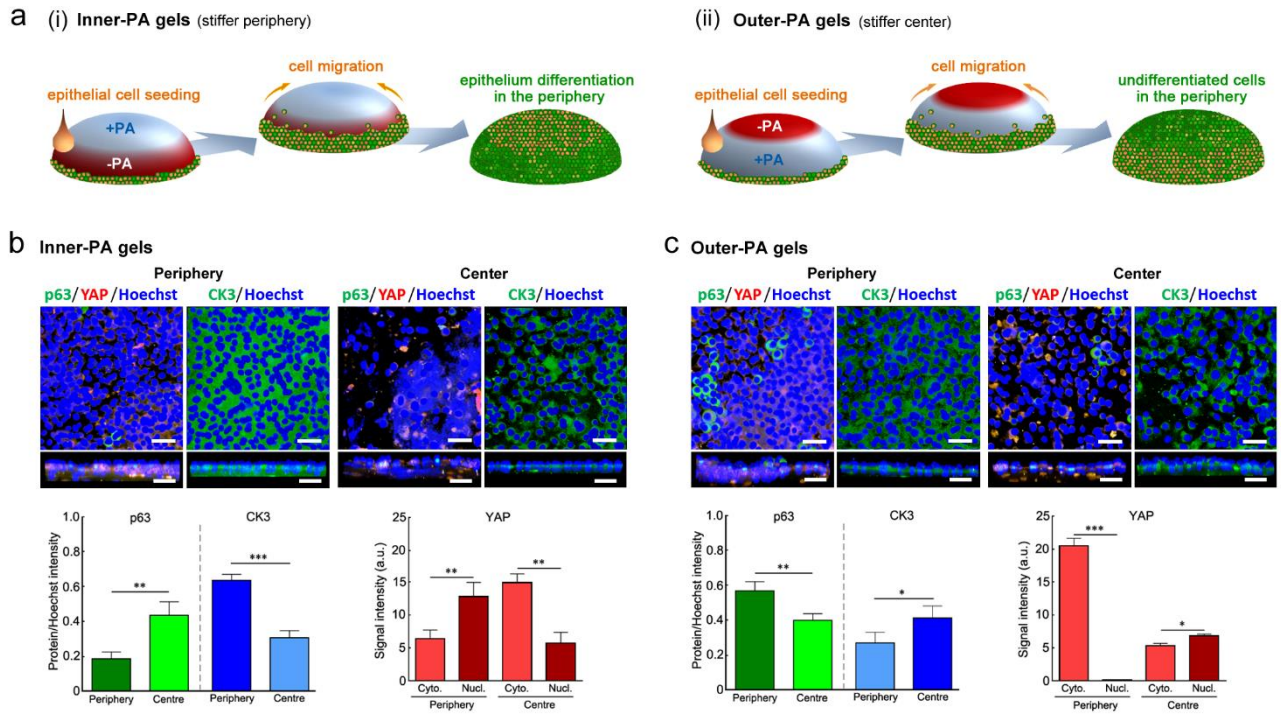

Figure 7: Self-curved gels used as substrates to support the growth and stratification of human limbal epithelial stem cells (epithelial cells). (a) Schematic depicting the seeding, migration, growth and differentiation/stratification of epithelial cells on self-curved (i) inner-PA and (ii) outer-PA gels. The impact of the substrate on the modulation of stem/progenitor cell (p63 and cytoplasmic YAP) and differentiation markers (CK3 and nuclear YAP) was evaluated by confocal immunofluorescence analysis (top and cross-section views) of both center and periphery of (b) inner-PA and (c) outer-PA gels after 10 days in culture. The detection of p63 (green)/YAP (red)/nuclei (blue), and of CK3 (green)/nuclei (blue) markers was quantified, with average± S.D. expression normalized to the intensity of nuclei signal in 10 independent gel locations (n = 1; *, ** and *** corresponded to $p < 0.05$, 0.01 and 0.001, respectively). Scale bars: 50 µm.

Graphical abstract